GRANT/TR/IN/25

Center for
Combustion and
Environmental
Research

COMBUSTION OF METALS IN REDUCED-GRAVITY AND EXTRATERRESTRIAL ENVIRONMENTS

M.C. Branch, A. Abbud-Madrid, and J. W. Daily

Center for Combustion and Environmental Research
Department of Mechanical Engineering
University of Colorado at Boulder
Boulder, CO 80309-0427

ANNUAL TECHNICAL REPORT
NASA Grant No. NAG-2220
October 10, 2001

Colorado
University of Colorado at Boulder

Introduction

As a result of the ongoing exploration of Mars and the several unmanned and possibly manned missions planned for the near future, increased attention has been given to the use of the natural resources of the planet for rocket propellant production and energy generation. Since the atmosphere of Mars consists of approximately 95% carbon dioxide (CO_2), this gas is the resource of choice to be employed for these purposes. Since many metals burn vigorously with CO_2, these may be used as an energy source or as propellants for a research vehicle on the surface of Mars. Shafirovich and Goldshleger[1] conducted experiments with spherical particles up to 2.5 mm in diameter and found that the burning process was controlled by diffusion and that the particles exhibited pulsating combustion due to superheating of the Mg vapor trapped inside a protective oxide shell. They also proposed a reaction mechanism based on the gas-phase reaction, $Mg + CO_2 \rightarrow MgO + CO$ and the heterogeneous reaction $Mg + CO \rightarrow MgO + C$ occurring on the sample surface.

In all the above studies with large Mg particles, the burning process is invariably influenced by strong convective currents that accelerate the combustion reaction and shorten the burning times. Although these currents are nearly absent in the burning of small particles, the high emissivity of the flames, rapid reaction, and small length scales make the gathering of any useful information on burning rates and flame structure very difficult. The goal of this investigation is to provide a detailed study of flame structure by taking advantage of large, free-floating spherical metal samples and their corresponding long burning times available in a weightless environment. The use of reduced gravity is essential to eliminate the intrusive buoyant flows that plague high-temperature metal reactions, to remove the destructive effect of gravity on the shape of molten

metal samples, and to study the combustion behavior of metals in the presence of solid oxides undisturbed by natural convection. This work presents the most complete modeling of metal particle burning to date for Mg with CO_2 and O_2.

Numerical Model

In the case of metal combustion experiments conducted in microgravity, a spherical symmetry during burning and the absence of natural-convection buoyant plumes are nearly achieved. The present experimental effort is complemented by the development of a numerical simulator, DROPLET, to model the spherically symmetric, quasi-steady burning of a metal fuel droplet with full gas-phase chemical kinetics and transport properties calculations. Due to the lack of kinetic and thermophysical data for the heterogeneous reactions of Mg and the absence of a complete condensation mechanism of MgO, the present model does not take into account surface reactions, radiation heat transfer, or complete condensation processes. Only vaporization of Mg from the sample surface is considered (with no heterogeneous surface reactions) and MgO condensation is treated with an Arrhenius-type rate expression for the molar production rate of the liquid, MgO(l) and solid oxide, MgO(s). The condensed products, MgO(l) and MgO(s), are treated like gas-phase species with a low diffusivity.

There are several numerical models already developed for the combustion of aluminum (Al) particles[2-5] that take into account some of the above processes not included in the present simulation. Unfortunately, these models can not be used in the case of Mg combustion since knowledge of the kinetic and thermophysical properties of Mg and its oxide is not as extensive as for Al. Thus, the present model was developed to help in the interpretation of the experimental

results and to serve as a preliminary effort for further development of a more complete and much needed model of Mg combustion.

Before attempting a Mg-CO_2 flame simulation, preliminary simulations of Mg-O_2 and Mg-air flames are performed since the reaction mechanisms for these systems are better understood. Equilibrium calculations by the NASA-Lewis chemical equilibrium code[6] are performed for all the above metal-oxidizer combinations to identify the most important species and to obtain the equilibrium temperature.

Mathematical Formulation

The one-dimensional conservation equations describing the quasi-steady burning of a spherical droplet in a quiescent gaseous atmosphere are:

$$\frac{1}{r^2}\frac{\partial}{\partial r}(r^2 \rho u_r) = 0 \tag{1}$$

$$\rho u_r C_P \frac{\partial T}{\partial r} = \frac{1}{r^2}\frac{\partial}{\partial r}(r^2 \lambda \frac{\partial T}{\partial r}) - \sum_{k=1}^{k_g} \rho Y_k V_k C_{P,k} \frac{\partial T}{\partial r} - \sum_{k=1}^{k_g} h_k \omega_k W_k \tag{2}$$

$$\rho u_r \frac{\partial Y_k}{\partial r} = -\frac{1}{r^2}\frac{\partial}{\partial r}(r^2 \rho Y_k V_k) + \omega_k W_k \tag{3}$$

The independent variable in these equations is the radial coordinate, r. The mass density, ρ, is calculated from the ideal-gas equation. The model assumes a uniform droplet temperature and the pressure is considered constant throughout the domain.

The multicomponent transport formulations are used for calculation of all transport properties. The species diffusion velocities are then expressed as:

$$V_k = \frac{1}{X_k \overline{W}} \sum_{j=1}^{k_g} W_j D_{kj} \frac{dX_j}{dr} - \frac{D_k^T}{\rho Y_k T} \frac{dT}{dr} \tag{4}$$

Boundary conditions

In order to solve the governing equations described above the following boundary conditions are imposed:

As $r \rightarrow \infty$:

$$Y_k = Y_{k,\infty}$$

$$T = T_\infty$$

At $r = r_s$:

$$\rho_s Y_{k,s} (u_r + V_k)_s = \omega_{k,s} W_k \tag{5}$$

$$\lambda_s (\frac{\partial T}{\partial r})_s = (\rho u_r)_s H_{fg} \tag{6}$$

$$Y_{f,s} = \frac{W_f}{\overline{W}} Exp[-\frac{H_{fg}}{R_f}(\frac{1}{T_s} - \frac{1}{T_b})] \tag{7}$$

Equation (5) is the species mass balance for the species at the surface implying that the chemical species flux at the surface is the same as the amount produced or destroyed by the surface chemical reaction. Equation (6) is the surface energy balance and Eq. (7) is the Clausius-Clapeyron liquid-vapor equilibrium relationship applied to the fuel.

In solving the above equations it is assumed that there is no reaction at the surface, so the right-hand side is zero in Eq. (5). Equation (1) can be simplified as:

$$r^2 \rho u_r = M_f \tag{8}$$

where the mass flux, M_f, is a constant. Thus, M_f is conserved throughout the domain. Use of this conserved scalar simplifies other governing equations. Hence, there is no need to solve for the velocity field.

Solution Method

Finite-difference approximations for non-uniform mesh spacing are used to solve the resulting system of partial differential equations by forming corresponding algebraic equations. Diffusive terms use central differences with truncation error that is second order in mesh spacing. For better convergence, convective terms use upwind differencing with truncation error that is first order in the mesh spacing. Use of Eq. (8) suggests that the resulting matrix structure is non-symmetric. Since TWOPNT[7], the boundary value problem solver used by this simulator, needs a block tridiagonal matrix structure, this equation is copied at each grid point. Also, no boundary condition is required for the mass flux far from the particle. The basic solution method is based on a damped modified Newton iteration. A time stepping algorithm is incorporated to help bring the successive iterations within the domain of convergence for Newton's method.

DROPLET is the simulator written for this specific problem. It uses CHEMKIN[8] and the transport package for kinetics and transport calculations, respectively. The flowchart of the simulator is shown in Fig. 1. The input to CHEMKIN consists of the reaction mechanism and the thermodynamic data. Input to the transport package is the transport property data. The CHEMKIN interpreter and the transport fitting code write respective linking files that can be retrieved by the corresponding libraries, such as CKLIB and TRANLIB. It also uses the boundary value problem solver, TWOPNT, to solve the resulting system of algebraic equations. The input file to DROPLET takes input from the user that consists of the pressure, initial number

of grid points, ambient (far field) conditions, and guessed values of surface and maximum temperatures. The output file written by DROPLET contains the initial guess and the final solution along with the intermediate solutions found on smaller grids.

Numerical Model Predictions

As explained in the Numerical Model section, numerical simulations are first conducted for the Mg-O_2 and Mg-air systems for which the reaction mechanisms are better understood. The reactions in the Mg-O_2 system are then used in the Mg-CO_2 simulation along with the reactions of Mg with CO_2 and CO, as well as all reactions of carbon-containing species with O_2 and O. For all three metal-oxidizer systems mentioned above, equilibrium calculations are performed with the NASA-Lewis chemical equilibrium code[6] to identify the most important species and to obtain the equilibrium temperature. For each of the three systems, it is necessary to include all three phases of MgO (gas, liquid, and solid) to obtain a realistic equilibrium temperature as observed in experiments. Including the gas- and liquid-phase species, MgO and MgO(l), as the only oxide products results in unrealistically low temperatures and species concentrations due to the absence of the large heat release experienced from the complete gas-to-solid condensation process. Hence, both the gas-to-liquid and liquid-to-solid condensation mechanisms must be considered for an accurate description of the Mg combustion process.

The Mg-O_2 flame structure

In the case of Mg-O_2, the equilibrium calculations are performed with 1 mole of gaseous Mg at 1366 K and 1 mole of O_2 at 300 K as the initial conditions. The equilibrium temperature

under adiabatic conditions is 3398 K and all three phases of MgO are present at this temperature. The numerical simulation of the Mg-O_2 flame structure uses the following reaction mechanism:

$$Mg + O_2 = MgO + O \quad (R1)$$

$$Mg + O + M = MgO + M \quad (R2)$$

$$MgO = MgO(l) \quad (R3)$$

$$MgO(l) = MgO(s) \quad (R4)$$

$$2O + M = O_2 + M \quad (R5)$$

Reactions (R1) and (R2) and their corresponding rate constants are determined from previous studies[9]. The symbol M represents the presence of a third body. The molar production rate of MgO(l) in reaction (R3) is obtained from the Arrhenius-type rate expression[10] of the condensation rate for the formation of drops of the critical radius (condensation nuclei) arising in a unit volume during a unit time. Due to the lack of a similar rate expression for the liquid-to-solid phase transition, a high value of the pre-exponential factor is used to simulate the condensation process of reaction (R4). This parameter is adjusted until a physically acceptable temperature profile is achieved. The condensed products are treated as gas-phase species with very low diffusivity. This is achieved by using a large value of the Lennard-Jones collision diameter in the transport property input. In the present simulations a Lennard-Jones collision diameter of 10 Å is chosen because is of the order of magnitude of the critical radius for condensation (3 Å) of MgO under the given conditions and small enough to avoid the treatment of a condensed phase. This value is used as a collision diameter for both MgO(l) and MgO(s). The rate constants for reactions (R1) through (R5) are shown in Table 1.

Figure 2 shows the flame structure of a 2-mm diameter Mg droplet burning in pure O_2 at 1 atm pressure and 300K temperature. Magnesium vapor diffuses out from the particle surface

towards the counterdiffusing O_2. The surface temperature is only a few degrees below the boiling point of Mg (1366K). The temperature profile rises with a very steep gradient near the surface to a short plateau region where a maximum temperature of 3220K is reached. After the complete consumption of the Mg vapor, the slope of the temperature profile starts decreasing at a faster rate. The predicted maximum temperature of 3220K is slightly lower than the maximum equilibrium temperature of 3398K, i. e. the vaporization-decomposition point of MgO under these conditions. This difference in maximum temperature values may be attributed to the lack of an accurate condensation model which may also be responsible for the absence of a large concentration of MgO(l) in the plateau region where the temperature exceeds the melting point of MgO (3105 K) and where the liquid oxide is the dominant species. The high pre-exponential factor used to simulate the liquid-to-solid phase change is insensitive to temperature and thus unable to simulate the rise of MgO(l) in the temperature plateau region. Hence only a very small amount of MgO(l) is obtained in the present calculations.

The gaseous oxide profile, MgO, shows a peak at the highest temperature and then rapidly decreases. As a result of the high flame temperature, a large amount of atomic oxygen, O, is also found in the plateau region of the temperature profile. The simulation also shows the diffusion of molecular oxygen, O_2, to the particle surface. Its significant concentration at the surface indicates that heterogeneous reactions may play an important role at the surface of the sample.

As mentioned before, the liquid and solid oxides are treated as gas-phase species with low diffusivity by using a Lennard-Jones collision diameter of 10 Å, a value of the same order of magnitude as the critical radius of condensation. To test the effectiveness of this approach, a collision diameter of 25 Å was used under the same conditions as in the original simulation. Under this higher collision diameter, the burning rate decreases by a factor of two and hence the

burning time increases by the same magnitude. Therefore, it appears that increasing the agglomeration of condensed products around the reaction zone results in increased hindrance to the transport of the gaseous oxidizer. However, since the estimate of burning times and hence the corresponding d^n law are strongly dependent on the assumed value of the collision diameter, no direct comparison with experimental burning times can be done without the inclusion of complete condensation and agglomeration mechanisms. Nevertheless, as will be seen in the following sections, comparisons can be done between burning rates obtained by simulation for the Mg-O_2, Mg-air, and Mg-CO_2 systems.

The Mg-Air flame structure

In the case of the Mg-air system, the equilibrium calculations are performed with 1 mole of gaseous Mg at 1366 K and 1 mole of air at 300 K as the initial conditions. The equilibrium temperature under adiabatic conditions is 3220 K with all three phases of MgO present at this temperature. For the numerical simulation of the Mg-air flame structure, nitrogen, N_2, is added (79% by volume) to the oxidizer to simulate the burning of Mg in air. The GRI-Mech™ 2.11 mechanism[11] is used to add the nitrogen chemistry to the Mg-O_2 mechanism. Other product species such as Mg_3N_2 and MgN are neglected in the present analysis due to the lack of kinetics and transport property information. The condensation of MgO into MgO(l) and MgO(s) is treated in the same manner as in the Mg-O_2 case. The reaction mechanism and rate constants for the Mg-air system are shown in Table 2.

Figure 3 shows the flame structure of a 2-mm diameter Mg droplet burning in air at 1 atm pressure and 300K temperature. As in the Mg-O_2 flame, the temperature profile rises sharply near the droplet surface. The maximum temperature in this case, however, is 3143 K, which is lower

than in the Mg-O_2 system due to the presence of N_2. This predicted maximum temperature of the Mg-air flame is also lower than the adiabatic flame temperature obtained in the equilibrium calculations (3220K) due to the lack of an accurate condensation model, which is also responsible for the absence of any significant concentration of MgO(l) in the temperature plateau region. The predicted burning rate is 1.5 times smaller than that obtained in the Mg-O_2 simulation. Also, an increase in the Lennard-Jones collision diameter to 25Å decreases the burning rate by a factor of two, which is in excellent quantitative agreement with the trend obtained in the simulation of Mg burning in pure oxygen.

The Mg-CO_2 flame structure

For the Mg-CO_2 system, an equilibrium calculation performed with 1 mole of gaseous Mg at 1366 K and 1 mole of CO_2 at 1000 K gives an equilibrium temperature under adiabatic conditions of 3174 K with all three phases of MgO present at this temperature. For the numerical simulation of the Mg-CO_2 flame structure, the reaction mechanism proposed by Shafirovich and Goldshleger[1] (described in the Introduction) is used for the reactions of Mg with CO_2 and CO:

$$Mg + CO_2 = MgO + CO \qquad (R11)$$

$$Mg + CO = MgO + C \qquad (R12)$$

The elementary steps and rate constants for reactions of carbon-containing species with O_2 and O are taken from the GRI-Mech™ 2.11 mechanism[11] and are shown in Table 3 along with all the Mg-O_2 and Mg-CO_2 reactions. Since the rate constants for reactions (R11) and (R12) are not well known, these constants are obtained for the present study from a sensitivity analysis and its comparison with experimental results. Species such as $MgCO_3$, MgC, and Mg_2C_3, predicted by

the equilibrium calculations, are neglected in the present analysis due to the lack of kinetics information. Condensation processes are treated in the same manner as in the Mg-O_2 and Mg-air cases.

The flame structure of a 2-mm diameter Mg droplet burning in a pure CO_2 atmosphere at 1 atm pressure is shown in Fig. 4. In this case the oxidizer ambient temperature is 1000 K since no convergence is obtained in the simulation for lower temperatures. This numerical result is in agreement with experimental studies[1] where the Mg sample is ignited by slowly heating the CO_2 gas around it. In these tests, no burning is obtained for ambient temperatures below 985 K. Under the experimental conditions used in the present investigation, the burning of the Mg sample under CO_2 ambient temperatures as low as 300 K is possible because enough radiant energy is provided to the sample to induce its ignition and subsequent burning before the energy source is turned off. The maximum combustion temperature predicted by the simulation is 2645 K, which is lower than the equilibrium temperature of 3174 K for CO_2 at an ambient temperature of 1000 K. The cause of this discrepancy in maximum temperature values follows the same reasoning as in the Mg-O_2 and Mg-air cases.

The reaction zone observed in Fig. 4 is narrower than in the Mg-O_2 and Mg-air simulations, suggesting a slower molecular diffusion process in the case of CO_2 as the oxidizer. This result is in qualitative agreement with the experiments where longer burning times are observed in Mg-CO_2 flames. The predicted burning rate is slightly lower than the rate obtained in the Mg-air simulation.

Conclusions

This investigation studies the burning behavior and flame structure of Mg in a CO_2 atmosphere to assess the feasibility of using metal-CO_2 reactions as an in situ resource utilization technology for rocket propulsion and energy generation on other planets. A one dimensional, spherically symmetric, quasi-steady model is used to simulate the burning behavior of Mg in O_2, air, and CO_2. The flame structure predicted by the model shows a temperature profile with a short plateau region at the highest temperature of the flame. It is within this region that the vaporization-dissociation of MgO takes place acting as an enthalpy sink. Condensation of MgO to MgO(l) and MgO(s) follows thereafter as it diffuses away from the flame. The maximum temperature obtained from the model is lower than that predicted by the equilibrium calculations and the high concentration of MgO(l) expected in the temperature plateau region is absent from the simulation results. Both effects are due to the lack of accurate information on the rates of liquid-to-solid condensation of the metal oxide.

In accordance with the experiments, the overall burning process appears to be diffusion controlled in all the cases. The burning rate and the maximum temperature in a CO_2 atmosphere are lower than in O_2 or air. For Mg burning in CO_2, an ambient temperature of 1000 K is necessary for convergence of the simulation, which agrees with experimental observations of samples ignited and burned by slow heating of the surrounding oxidizer.

At the present time, this preliminary model does not give a complete picture of the metal-oxidizer reaction since not all of the relevant physical and chemical mechanisms are considered. Product condensation and agglomeration, radiation heat loss, and heterogeneous surface reactions are just some of the important mechanisms that should be included in the model to provide an accurate representation of the burning process. In addition, there is also a lack of information in

the literature on reaction rates of the most basic elementary reactions. Nevertheless, although preliminary, the model provides a qualitative description of the flame structure that helps to visualize the complex phenomenon of metal combustion.

References

1. Shafirovich, E. Ya. and Goldshleger, U. I., "Combustion of Magnesium Particles in CO_2/CO Mixtures," *Combustion, Science, and Technology*, Vol. 84, 1992, pp. 33-43.

2. Law, C. K., "A Simplified Theoretical Model for the Vapor-Phase Combustion of Metal Particles," *Combustion, Science, and Technology*, Vol. 7, 1973, pp. 197-212.

3. King, M. K., "Modeling of Single Particle Aluminum Combustion in CO_2-N_2 Atmospheres," *Seventeenth Symposium (International) on Combustion,* The Combustion Institute, Pittsburgh, 1979, pp. 1317-1328.

4. Brooks, K. P. and Beckstead, M. W., "Dynamics of Aluminum Combustion," *Journal of Propulsion and Power*, Vol. 11, 1995, pp. 769-780.

5. Bucher, P., Yetter, R. A., Dryer, F. L., Parr, T. P., Hanson-Parr, D. M., "PLIF Species and Ratiometric Temperature Measurements of Aluminum Particle Combustion in O_2, CO_2 and N_2O oxidizers, and Comparison with Model Calculations," *Twenty-Seventh Symposium (International) on Combustion,* The Combustion Institute, Pittsburgh, 1998, pp. 2421-2429.

6. McBride, B. J. and Gordon, S., "Computer Program for Calculation of Complex Chemical Equilibrium Compositions and Applications," NASA Lewis Research Center, Reference Publication 1311, Cleveland, OH, 1996.

7. Grcar, J. F., "The Twopnt Program for Boundary Value Problems," Sandia National Laboratories, Report SAND91-8230, Livermore, CA,1992.

8. Kee, R. J., Miller, J. A., and Jefferson, T. H., "CHEMKIN: A General-Purpose, Problem-Independent, Transportable, Fortran Chemical Kinetics Code Package," Sandia National Laboratories, Report SAND80-8003, Livermore, CA, 1980.

9. Mellor, A. M., Wittig, S. L. K., and Whitacre, R. F., "Spectrometric Study of Shock-Heated Mg/MgO Particle Dispersions," *Combustion, Science, and Technology*, Vol. 4, 1971, pp. 31-36.

10. Pilyugin, N. N., "Nonequilibrium Magnesium-Related Processes in the Wake behind a Model Moving with Hypersonic Speed in Air," *Combustion, Explosion, and Shock Waves,* Vol. 36, 2000, pp. 349-357.

11. Bowman, C.T., Hanson , R.K., Gardinger Jr., W.C., Lissianski, V., Frenklach, M., Goldenberg, M., and Smith, G.P., "GRI-Mech-An Optimized Detailed Chemical Reaction Mechanism for Methane Combustion and NO Formation and Reburning," Gas Research Institute, Report No. 97-0020, 1997.

12. Tsang, W., Hampson, R.F. "Chemical Kinetic Database for Combustion Chemistry," *Journal of Physical Chemistry Reference Data*, Vol. 15, 1986, p. 1087.

Students Supported

1. Abhijit Modak, PhD., in progress
2. Robyn Wing, Undergraduate Research Intern
3. Heather Alberts, Undergraduate Research Intern

Publications and Presentations

1. Modak, A. Abbud-Madrid, M. C. Branch, and J. W. Daily, "Combustion of Magnesium with Carbon Dioxide and Carbon Monoxide at Low Gravity," Journal of Propulsion and Power, 17, pp.852-859, 2001.

2. B. Dreyer, J. W. Daily, A. Abbud-Madrid, M. C. Branch, "Laser Induced Fluorescence Excitation Spectroscopy of Magnesium Oxide," Applied Optics, in press.

3. C.B. Dreyer, J.W. Daily, A. Abbud-Madrid, and M.C. Branch, "Planar Laser Induced Fluorescence Measurements of Magnesium Oxide During Combustion of Magnesium with Oxygen and Carbon Monoxide, AIAA Aerospace Sciences Meeting, Reno, January 8-11, 2001.

4. Modak, A. Abbud-Madrid, M.C. Branch, "A Comprehensive Model of Combustion of Mg Particles in CO2, O2 and Air," 29th Symposium (International) on Combustion, the Combustion Institute, in preparation.

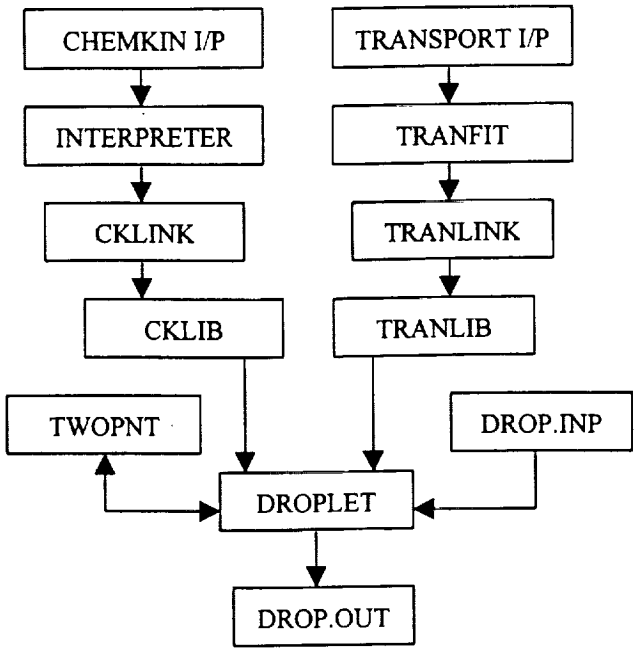

Figure 1. Flowchart of the DROPLET numerical simulator.

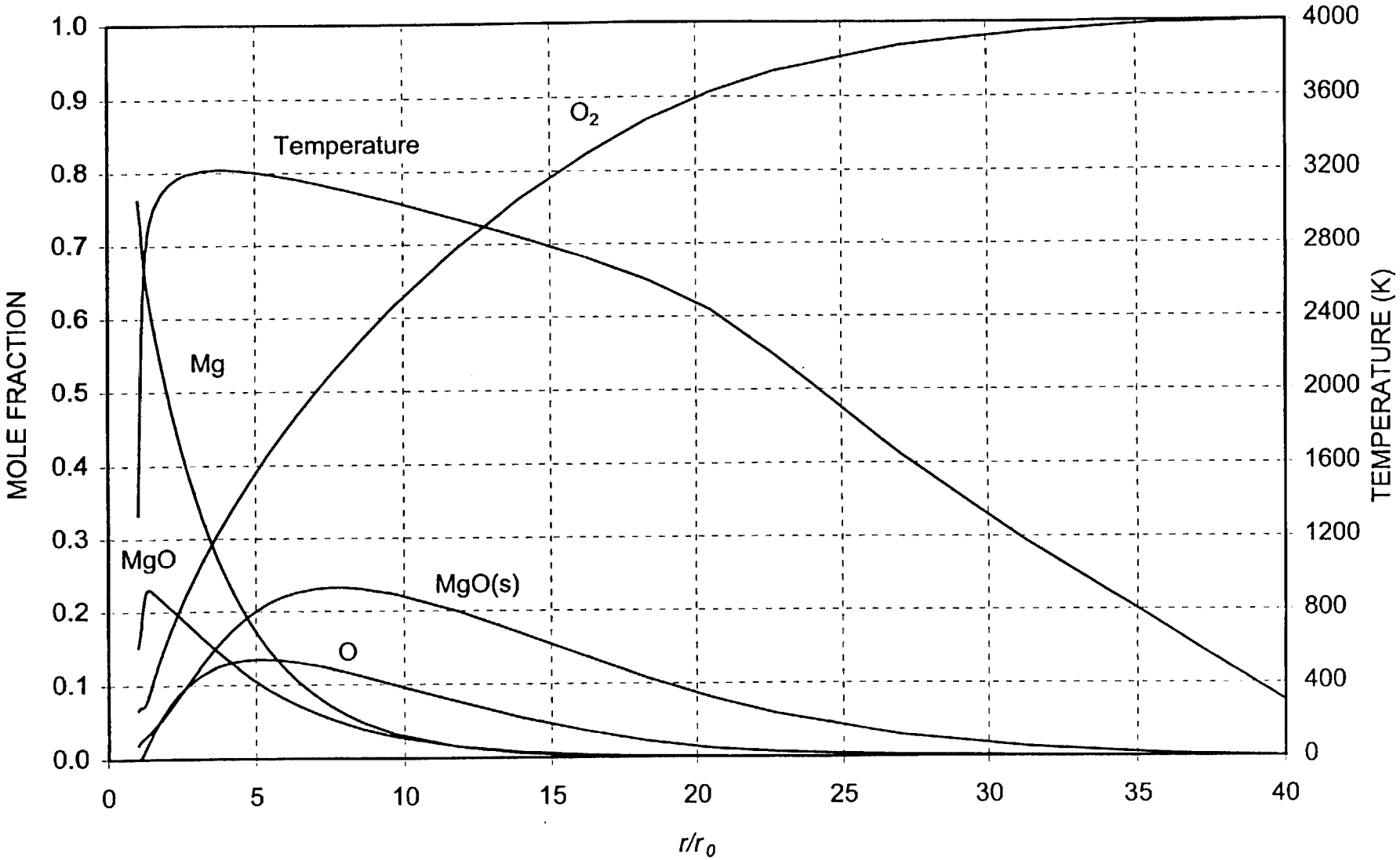

Figure 2. Flame structure of a 2-mm diameter Mg droplet burning in O_2 obtained with the DROPLET numerical simulator.

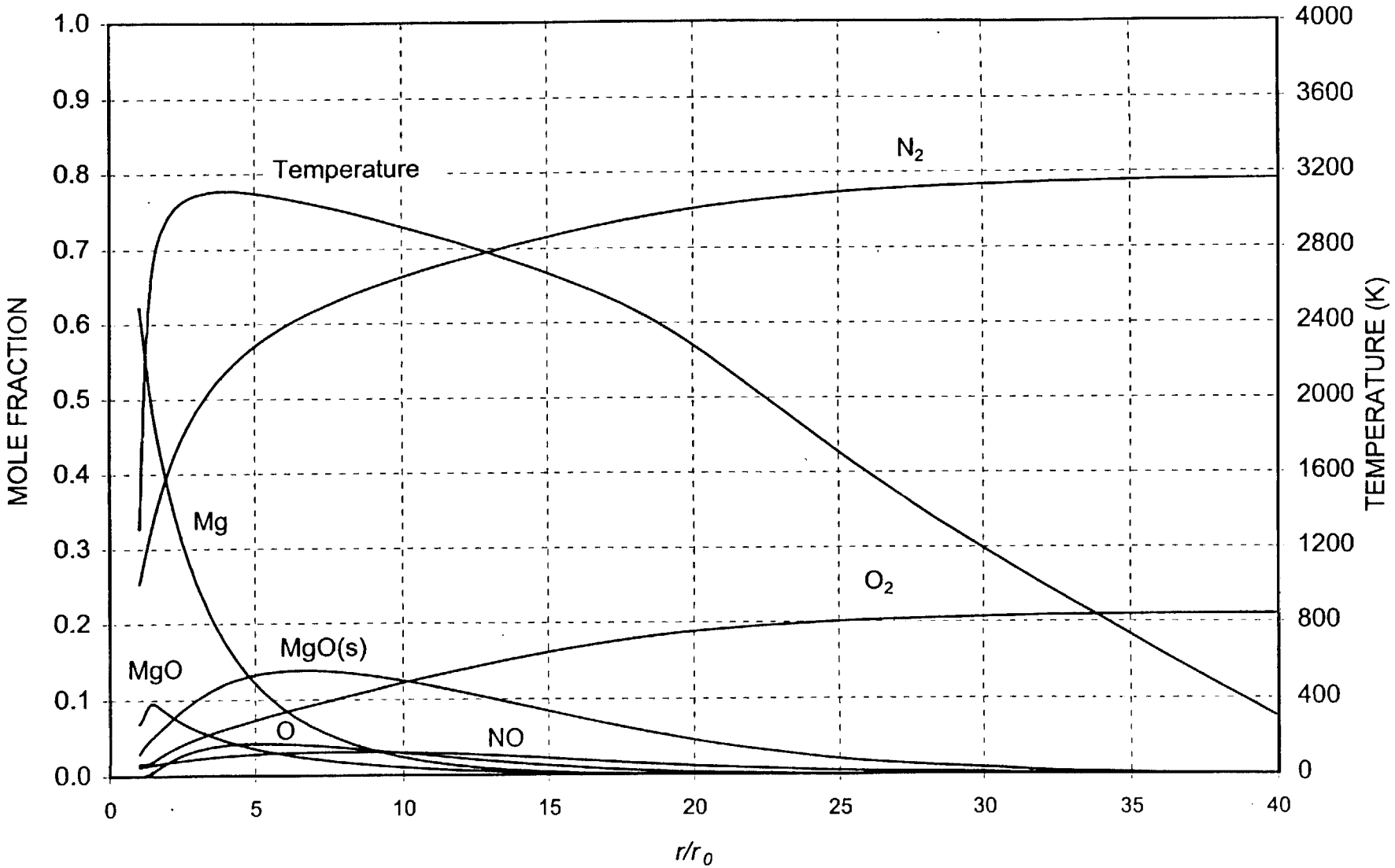

Figure 3. Flame structure of a 2-mm diameter Mg droplet burning in air obtained with the DROPLET numerical simulator.

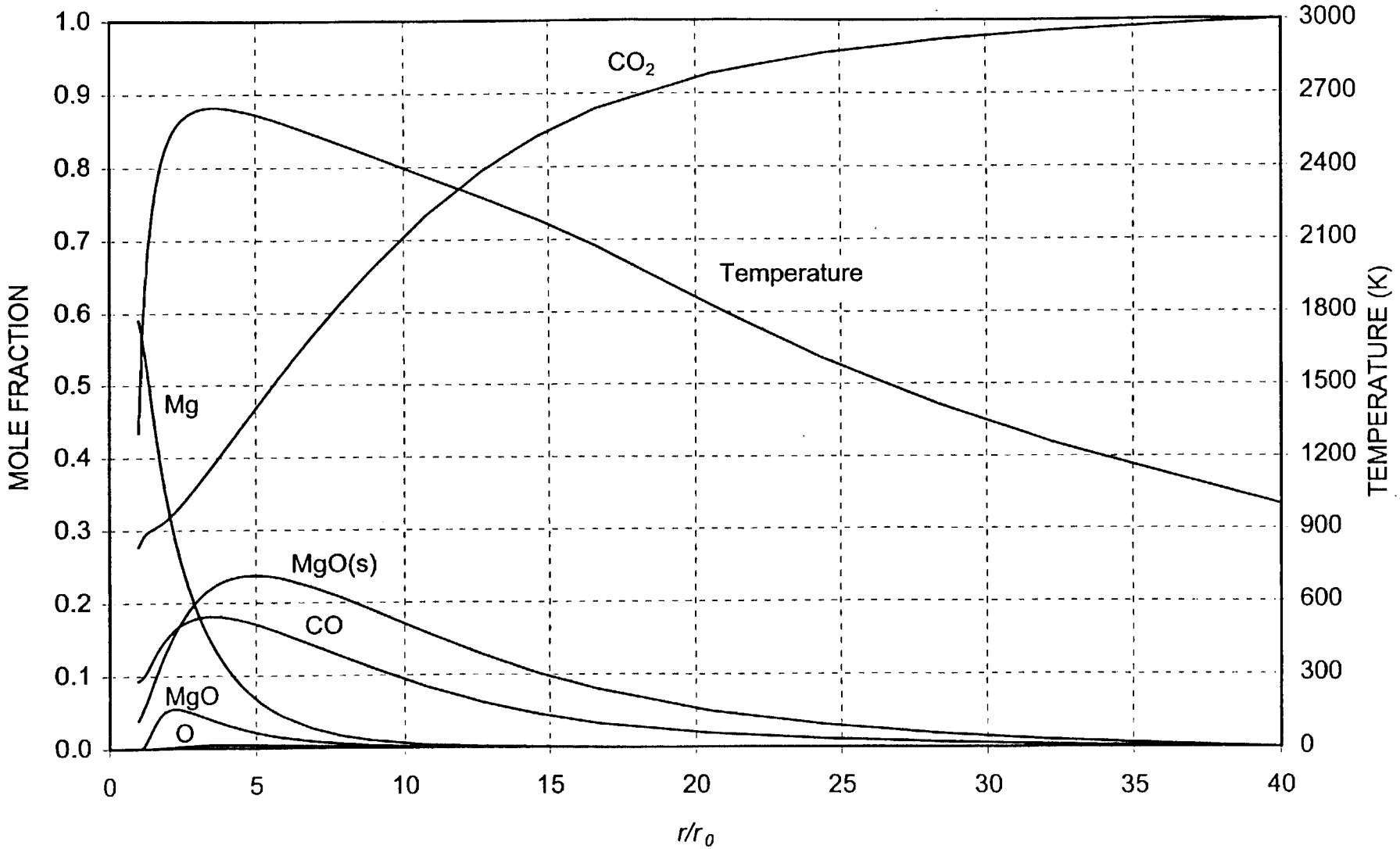

Figure 4. Flame structure of a 2-mm diameter Mg droplet burning in CO_2 obtained with the DROPLET numerical simulator.

Table 1. Reaction Mechanism for $Mg\text{-}O_2$

Reaction		A	β	E_A	Ref.
$Mg + O_2 = MgO + O$	(R1)	4.44E+12	0.5	30500.0	9
$Mg + O + M = MgO + M$	(R2)	1.90E+14	0.5	0.0	9
$MgO = MgO(l)$	(R3)	6.11E+11	-2.0	17268.6	10
$MgO(l) = MgO(s)$	(R4)	1.00E+15	0.0	0.0	--
$2O + M = O_2 + M$	(R5)	1.89E+13	0.0	-1788.0	12

The rate coefficients are in the form $K_j = A*T^{\beta} Exp(-E_A/RT)$. Units are in moles, cubic centimeters, seconds, Kelvins, and calories/mole.

Table 2. Reaction Mechanism for Mg-Air

Reaction		A	β	E_A	Ref.
$Mg + O_2 = MgO + O$	(R1)	4.44E+12	0.5	30500.0	9
$Mg + O + M = MgO + M$	(R2)	1.90E+14	0.5	0.0	9
$MgO = MgO(l)$	(R3)	6.11E+11	-2.0	17268.6	10
$MgO(l) = MgO(s)$	(R4)	1.00E+15	0.0	0.0	--
$2O + M = O_2 + M$	(R5)	1.89E+13	0.0	-1788.0	12
$N + NO = N_2 + O$	(R6)	3.50E+13	0.0	330.0	11
$N + O_2 = NO + O$	(R7)	2.65E+12	0.0	6400.0	11
$N_2O + O = N_2 + O_2$	(R8)	1.40E+12	0.0	10810.0	11
$N_2O + O = 2NO$	(R9)	2.90E+13	0.0	23150.0	11
$NO_2 + O = NO + O_2$	(R10)	3.90E+12	0.0	-240.0	11

The rate coefficients are in the form $K_j = A*T^{\beta} Exp(-E_A/RT)$. Units are in moles, cubic centimeters, seconds, Kelvins, and calories/mole.

Table 3. Reaction Mechanism for Mg-CO_2

Reaction		A	β	E_A	Ref.
$Mg + CO_2 = MgO + CO$	(R11)	2.00E+14	0.5	34847.0	1
$Mg + CO = MgO + C$	(R12)	2.00E+11	0.5	30000.0	1
$Mg + O_2 = MgO + O$	(R1)	4.44E+12	0.0	30500.0	9
$Mg + O + M = MgO(s) + M$	(R2)	1.90E+14	0.0	0.0	9
$MgO = MgO(l)$	(R3)	6.11E+11	-2.0	17268.6	10
$MgO(l) = MgO(s)$	(R4)	1.00E+15	0.0	0.0	--
$2O + M = O_2 + M$	(R5)	1.89E+13	0.0	-1788.0	12
$CO + O + M = CO_2 + M$	(R13)	6.02E+14	0.0	3000.0	11
$CO + O_2 = CO_2 + O$	(R14)	2.50E+12	0.0	47800.0	11
$C + O_2 = CO + O$	(R15)	5.80E+13	0.0	576.0	11

The rate coefficients are in the form $K_j = A*T^{\beta} Exp(-E_A/RT)$. Units are in moles, cubic centimeters, seconds, Kelvins, and calories/mole.

Publications and Presentations

1. Modak, A. Abbud-Madrid, M. C. Branch, and J. W. Daily, "Combustion of Magnesium with Carbon Dioxide and Carbon Monoxide at Low Gravity," Journal of Propulsion and Power, 17, pp.852-859, 2001.

2. B. Dreyer, J. W. Daily, A. Abbud-Madrid, M. C. Branch, "Laser Induced Fluorescence Excitation Spectroscopy of Magnesium Oxide," Applied Optics, in press.

3. C.B. Dreyer, J.W. Daily, A. Abbud-Madrid, and M.C. Branch, "Planar Laser Induced Fluorescence Measurements of Magnesium Oxide During Combustion of Magnesium with Oxygen and Carbon Monoxide, AIAA Aerospace Sciences Meeting, Reno, January 8-11, 2001.

4. Modak, A. Abbud-Madrid, M.C. Branch, "A Comprehensive Model of Combustion of Mg Particles in CO2, O2 and Air," 29th Symposium (International) on Combustion, the Combustion Institute, in preparation.

Table 1. Reaction Mechanism for Mg-O_2

Reaction		A	β	E_A	Ref.
$Mg + O_2 = MgO + O$	(R1)	4.44E+12	0.5	30500.0	9
$Mg + O + M = MgO + M$	(R2)	1.90E+14	0.5	0.0	9
$MgO = MgO(l)$	(R3)	6.11E+11	-2.0	17268.6	10
$MgO(l) = MgO(s)$	(R4)	1.00E+15	0.0	0.0	--
$2O + M = O_2 + M$	(R5)	1.89E+13	0.0	-1788.0	12

The rate coefficients are in the form $K_j = A*T^{\beta} Exp(-E_A/RT)$. Units are in moles, cubic centimeters, seconds, Kelvins, and calories/mole.

Table 2. Reaction Mechanism for Mg-Air

Reaction		A	β	E_A	Ref.
$Mg + O_2 = MgO + O$	(R1)	4.44E+12	0.5	30500.0	9
$Mg + O + M = MgO + M$	(R2)	1.90E+14	0.5	0.0	9
$MgO = MgO(l)$	(R3)	6.11E+11	-2.0	17268.6	10
$MgO(l) = MgO(s)$	(R4)	1.00E+15	0.0	0.0	--
$2O + M = O_2 + M$	(R5)	1.89E+13	0.0	-1788.0	12
$N + NO = N_2 + O$	(R6)	3.50E+13	0.0	330.0	11
$N + O_2 = NO + O$	(R7)	2.65E+12	0.0	6400.0	11
$N_2O + O = N_2 + O_2$	(R8)	1.40E+12	0.0	10810.0	11
$N_2O + O = 2NO$	(R9)	2.90E+13	0.0	23150.0	11
$NO_2 + O = NO + O_2$	(R10)	3.90E+12	0.0	-240.0	11

The rate coefficients are in the form $K_j = A*T^{\beta} Exp(-E_A/RT)$. Units are in moles, cubic centimeters, seconds, Kelvins, and calories/mole.

Table 3. Reaction Mechanism for $Mg\text{-}CO_2$

Reaction		A	β	E_A	Ref.
$Mg + CO_2 = MgO + CO$	(R11)	2.00E+14	0.5	34847.0	1
$Mg + CO = MgO + C$	(R12)	2.00E+11	0.5	30000.0	1
$Mg + O_2 = MgO + O$	(R1)	4.44E+12	0.0	30500.0	9
$Mg + O + M = MgO(s) + M$	(R2)	1.90E+14	0.0	0.0	9
$MgO = MgO(l)$	(R3)	6.11E+11	-2.0	17268.6	10
$MgO(l) = MgO(s)$	(R4)	1.00E+15	0.0	0.0	--
$2O + M = O_2 + M$	(R5)	1.89E+13	0.0	-1788.0	12
$CO + O + M = CO_2 + M$	(R13)	6.02E+14	0.0	3000.0	11
$CO + O_2 = CO_2 + O$	(R14)	2.50E+12	0.0	47800.0	11
$C + O_2 = CO + O$	(R15)	5.80E+13	0.0	576.0	11

The rate coefficients are in the form $K_j = A*T^{\beta} Exp(-E_A/RT)$. Units are in moles, cubic centimeters, seconds, Kelvins, and calories/mole.